Theoretical Stability Derivatives for a Ducted Propeller

ANTHONY R. KRIEBEL*
Itek Corporation, Palo Alto, Calif.

In the present paper the static force and moment coefficients at angle of attack and their dynamic pitching derivatives are given for an isolated ducted propeller. These result from a potential flow analysis that is based upon Fourier expansion of the vorticity distribution. The analysis offers a valid technique for combining existing theory for ring wings at angle of attack and ducted propellers in axial flow. The propeller is represented as a uniformly loaded actuator disk, and the effects of duct chord-to-diameter ratio, circular arc camber, taper, and thickness are shown for the duct coefficients and their pitching derivatives. The details of the mathematical development appear in the comprehensive Vidya Technical Report 112. The static coefficients reduce to those previously obtained by Burrgraf for a short, thin, cylindrical duct and uniform actuator disk; and when both the actuator disk loading and free-stream angle of attack become small, the coefficients reduce to those obtained by Weissinger for a ring wing. The new results consist of the static coefficients and the dynamic pitching derivatives for a duct with camber, taper, thickness, and increased chord.

Nomenclature

A = area of duct exit plane, $\pi D^2/4$
A_p = actuator disk area equal to local internal cross-sectional area of duct, $\pi D_p^2/4$
C_m = pitching moment coefficient, $2M/DAq_0$
C_N = normal-force coefficient, N/Aq_0
$C_{T_{P(D)}}$ = thrust coefficient of propeller or actuator disk, $T_{P(D)}/A_pq_0$
C = duct force or moment coefficient or stability derivative, Eqs. (5–8), and Eqs. (10–13), e.g., $C_{m_\alpha} = \partial C_m/\partial\alpha$, $C_{m_q} = \partial C_m/\partial(Dq/V_0)$, $C_{m_{\dot\alpha}} = \partial C_m/\partial(D\dot\alpha/V_0)$
c = chord length of duct
D = diameter of thin cylindrical duct and actuator disk, or diameter of exit plane for duct with thickness, camber, or taper
D_p = propeller diameter for duct with thickness, camber, or taper; for thin cylindrical duct $D_p = D$
f_n = functions of c/D, Eqs. (5–13)
$M_{D(P)}$ = aerodynamic pitching moment on the duct in the presence of a propeller represented as an actuator disk; positive clockwise in Fig. 1 about the duct midchord diameter
$N_{D(P)}$ = normal-force component on the duct in the presence of a propeller, Fig. 1
Δp = actuator disk loading or pressure jump
q = pitching rate, rad/sec, Fig. 1
q_0 = freestream dynamic pressure, $(\frac{1}{2})\rho V_0^2$
R = duct radius, $D/2$
R_1, R_2 = duct shape coefficients, Eq. (14)
r_s, x_s = coordinates of surface of cambered or tapered duct, Fig. 6
V_0 = freestream velocity, Fig. 1
V_x, V_z = axial and radial components of V_0, Fig. 1
V_j = axial velocity component in slipstream, Fig. 1
α_0 = freestream angle of attack, rad, Fig. 1
ρ = fluid density, slug/ft^3
τ = maximum duct profile thickness is τc

Subscripts

DP = ducted actuator disk combination
$D(P)$ = duct in the presence of a propeller represented as a uniformly loaded actuator disk
h = hovering flight condition with $V_0 = q = 0$
N = component of moment due to N
$P(D)$ = propeller represented as a uniformly loaded actuator disk, shrouded by a duct
T = component of moment due to T

Presented as Preprint 64-170 at the AIAA General Aviation Aircraft Design and Operations Meeting, Wichita, Ka., May 25–27, 1964; revision received May 5, 1964. This work was supported by Bureau of Naval Weapons, Department of the Navy, under Contract NOw 62-0129-c, and was administered under technical direction of the Fluid Mechanics and Flight Dynamics Branch, RRRE-4.

* Staff Scientist, Aerodynamics, Vidya Division. Member AIAA.

1. Introduction

BY adding a duct or shroud to a propeller one can generate a thrust force on the duct and increase the flow rate through the propeller during axial flight and particularly during hovering flight. If the propeller is properly designed to operate within the duct, the propulsive efficiency can increase with the flow rate for the same total thrust force on the duct and propeller. Furthermore, the decreased loading on the propeller blades can alleviate compressibility effects, cavitation, and noise generation.

At angle of attack, the ducted propeller generates much more lift force than an open propeller. Because of mutual interference the lift force on the ducted propeller can be even larger than on a ring wing and propeller that are separated from each other. The relatively large lift and thrust forces that can be generated by a ducted propeller, as compared with an open propeller of equal diameter, make it an attractive device for use on VTOL aircraft.

The benefits of increasing the flow rate by ducting a propeller were first demonstrated in 1931 by the experiments of Stipa in Italy and in 1940 by the analysis of Dickmann in Germany.[1] In recent years with the advent of hovering flight, vertical takeoff, and sustained travel underwater, ducted propellers have received considerable attention, particularly by experimental investigators as reviewed in Ref. 2.

Because of its mathematical complexity, the analysis of the ducted propeller has lagged far behind experiment. However, a rigorous, self-consistent theory is now emerging for steady axial flow.[3–5] This theory is based upon the classical method of singularities in three dimensions and is restricted to light duct and propeller loading (i.e., small perturbations).

An approximate theory for steady flow at angle of attack has been developed by Burggraf[6] where the ducted propeller

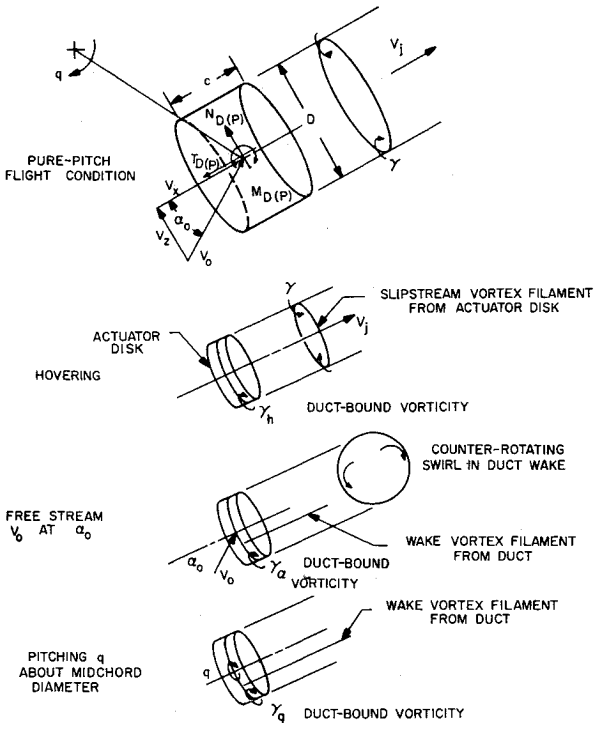

Fig. 1 Nomenclature for pure-pitch flight condition.

is represented as a short, thin, cylindrical duct with a uniformly loaded actuator disk across its exit plane. This analysis has been extended in Ref. 7 to include pitching and plunging motions and propellers with finite blades, where a comparison with the applicable experimental data and a calculative example of the over-all dynamic characteristics of a torpedo-like hull with a ducted propeller are also given.

An analysis has been made of an isolated ducted propeller of less restricted shape than that described in Refs. 6 and 7. The results of this analysis are summarized herein. These results will be compared with the approximate relations previously obtained for short cylindrical ducts. Included in this paper are the duct-to-disk thrust ratio for hovering and axial flight, the force and moment coefficients of the duct for steady flight at angle of attack, and the stability derivatives of the duct for pitching motion. The results are given first for a duct that is thin and cylindrical but not necessarily short. The effects of duct camber, taper, and thickness are then considered.

The analysis makes extensive use of previous analytical results for an isolated ring wing,[8–10] and a ducted propeller, [1, 4, 5, 11] but differs from these analyses in the following respects. The effects of an actuator disk and pitching motion are incorporated into the analysis of Refs. 8–10; furthermore, since the ducted actuator disk is not restricted to small angles of attack and light loading, the axial velocity self-induced by the duct vorticity is not neglected. The effect of pitching motion is added in Ref. 1. Axial flow and light loading are not assumed as in Refs. 4, 5, and 11. References 4 and 5 include the effects of finite propeller blades with nonuniform blade loading and tip clearance, which are not considered here.

2. Method of Approach

The results to be given were obtained by analysis of the flow model shown in Fig. 1. The aerodynamic force and moment acting on the duct in the presence of the propeller are found by assuming the duct to be a thin cylinder and by representing the propeller as a uniformly loaded actuator disk. The disk is located at the duct inlet for convenience, since the results for a thin cylindrical duct are independent of disk location within the duct.[7] For ducts with camber, taper, or thickness, the disk location is an important variable as shown in Sec. 4.

By the method of singularities the vorticity distribution bound to the duct and trailing from it is found in terms of a Fourier series for the "pure pitch" flight condition shown in Fig. 1. A boundary condition is imposed and the Kutta-Joukowski condition is satisfied by specifying that there be no flow through the duct surface or across its trailing edge. The pure pitch flow field is composed of the three additive components shown in Fig. 1: 1) that induced by the actuator disk for hovering flight with $V_0 = q =$ zero; 2) that generated by the freestream V_0 at angle of attack α_0 over the duct alone (or ring wing); and 3) that for the duct alone, because of its pitching motion, or angular velocity q about the midchord diameter perpendicular to V_0. It can be seen that the pure pitch flow field is equivalent to that for a ducted actuator disk mounted at angle α_0 on an arm of radius V_0/q rotating through still fluid with angular velocity q.

The three flow fields are additive because of the analytical assumption that all of the vorticity shed by both the actuator disk and the duct is always concentrated on a circular cylinder which extends axially downstream, even at angle of attack, as in Refs. 1 and 11. Since the three flow fields are

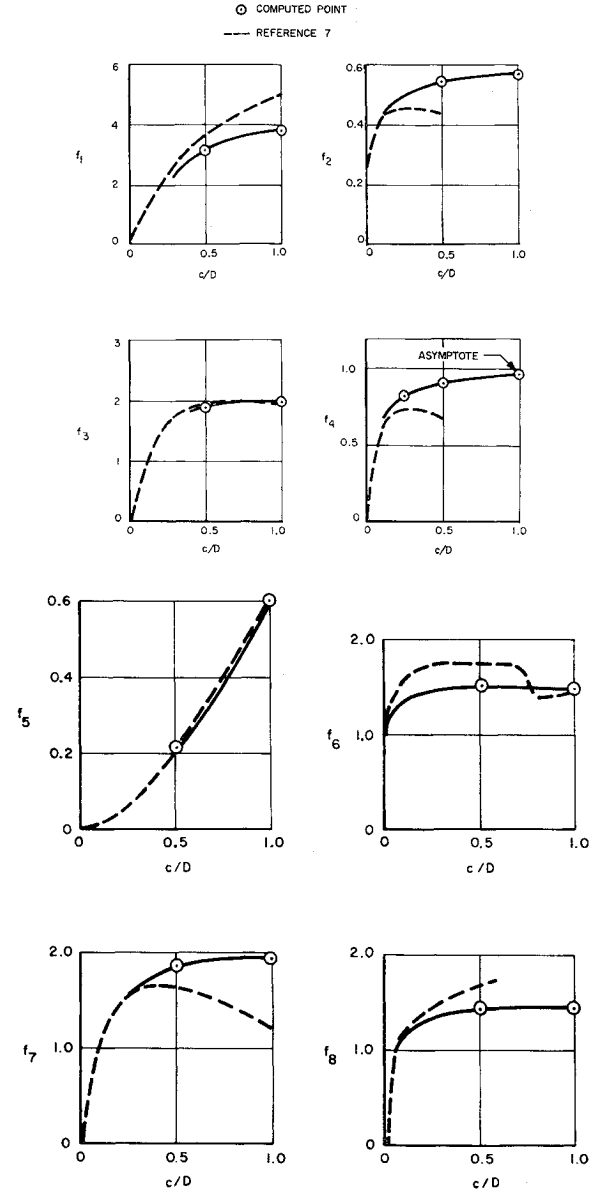

Fig. 2 Computed functions of duct chord-to-diameter ratio, Eqs. (5–9), Table 1.

additive, existing ducted-propeller theory can be used to obtain the first flow-field component, and existing ring-wing theory to obtain the second two components. Because of the assumptions regarding the wake, the actuator disk loading must be large at high angles of attack in order to produce a high-velocity slipstream that remains nearly aligned with the duct axis. In other words, the slipstream velocity must be large compared with the cross-flow component of the freestream, or $V_j \gg V_0 \sin\alpha_0$. We also assume that the vortex cylinder shed by the disk is of constant strength γ as in Refs. 1, 6, 7, and 11. This assumption is more valid for a ducted propeller than an isolated propeller.

The analysis assumes that the fluid is inviscid and incompressible. The duct boundary layer, frictional drag, and the possibility of flow separation are not considered here, but the boundary layer has been considered previously for a ring wing.[10, 12]

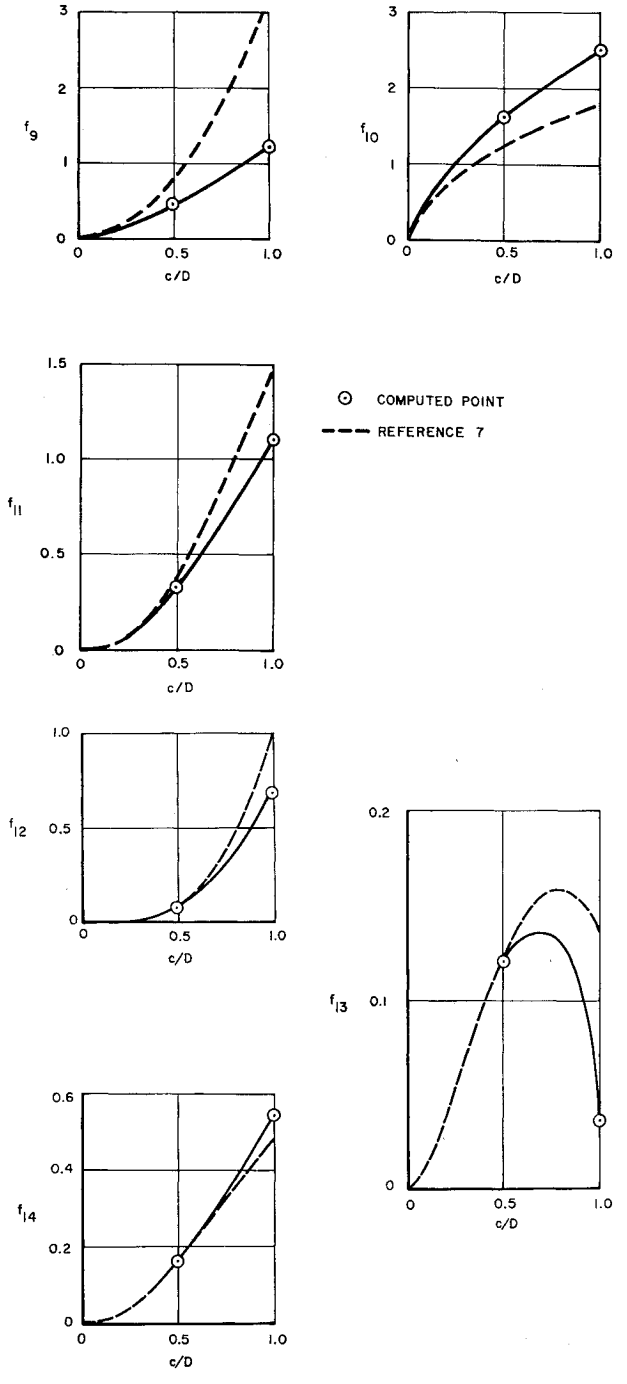

Fig. 3 Computed functions of duct chord-to-diameter ratio, Eqs. (10–13), Table 1.

For any combination of the three flow fields, the net force and moment on the duct is found by integration of the surface pressure distribution including the leading-edge singularity. For the freestream at angle of attack and with no pitching motion, the static force and moment coefficients are obtained. In the detailed analysis[18] the pitching derivatives are found from the pure pitch flight condition by the following procedure. For the pure pitch flight condition it is found that the force and moment coefficients are all proportional to the pitch rate q except for the thrust force coefficient. Partial differentiation of the force and moment coefficients with respect to q, holding V_0, γ, and α_0 constant gives the stability derivatives due to pitch which are given herein. In the final expression for the pitching derivative of the thrust coefficient, q is set equal to zero. Thus, except for the thrust coefficient, the duct force and moment coefficients due to pitch are equal to the pitching derivatives given herein times Dq/V_0, the dimensionless pitch rate.

The duct force is composed of two components, axial thrust and normal force. The duct pitching moment is about the duct midchord diameter (Fig. 1) and is composed of components due to the thrust and normal force.

The coefficients and pitching derivatives for a thin cylindrical duct depend upon only the chord-to-diameter ratio of the duct c/D, the angle of attack α_0, and the ratio γ/V_0 that is expressed in terms of the propeller thrust coefficient.

The present analysis gives the force and moment of the duct in the presence of an actuator disk with a specified uniform loading. The forces and moments on a propeller having finite blades and located within a duct are considered in Ref. 7 and shown to be negligibly small compared with those on a duct (with $c = 0.2D$), except for the propeller thrust force and the pitching moment on the propeller due to pitching motion. Duct interference on the propeller can markedly effect the latter moment to increase the damping of the pitching motion.[7]

Since the pure pitch motion is steady in time, the apparent mass or plunging ($\dot{\alpha}$) derivatives are not given by the present analysis. A formula for the apparent mass of a short duct is given in Ref. 7, however. Calculative examples for typical torpedo and VTOL configurations in the comprehensive report from which the present results are taken[18] indicated that the apparent mass of the ducted propellers for such vehicles probably do not damp their motion appreciably, that is, there is little contribution to $C_{m_q} + C_{m_{\dot{\alpha}}}$.

Summarizing the initial assumptions described above, we have 1) a thin cylindrical duct with a uniformly loaded actuator disk of equal diameter, 2) potential flow steady in time, 3) constant actuator disk vorticity γ, and 4) $V_j \gg V_0 \sin\alpha_0$, with all trailing vorticity placed on a circular cylinder aligned with the duct axis, so that various flow fields can be added to form the pure pitch flight condition.

3. Analytical Results for a Thin Cylindrical Duct

The results for forces, moments, and stability derivatives were obtained by solving for the coefficients of Fourier series representing the duct-bound vorticity distribution. The solution utilizes influence coefficients which have been machine computed and listed in Refs. 5 and 10. Since the complete set of coefficients is available only for duct chord-to-diameter ratios of 0.5 and 1.0, most of the results presented herein are given only for these two values. For axial flow the coefficients are also available for chord-to-diameter ratios of 0.25, 0.75, 1.5, and 2.0. However, with the linearized analysis of Ref. 7 for small chord-to-diameter ratios, the results of which are plotted as dashed lines in Figs. 2 and 3, one can interpolate to obtain the stability derivatives for a duct having any chord-to-diameter ratio within the range of practical interest.

Table 1 Computed functions of duct chord-to-diameter ratio for a thin cylindrical duct

c/D	0.5	1.0
f_1	3.075	3.694
f_2	0.530	0.552
f_3	1.893	1.988
f_4	0.916	0.967
f_5	0.214	0.598
f_6	1.499	1.466
f_7	1.862	1.961
f_8	1.437	1.434
f_9	0.428	1.195
f_{10}	1.602	2.455
f_{11}	0.329	1.104
f_{12}	0.074	0.664
f_{13}	0.120	0.037
f_{14}	0.162	0.544

The static coefficients and stability derivatives depend on the ratio of the vorticity shed from the actuator disk and the freestream velocity γ/V_0. This ratio can be expressed in terms of the actuator disk loading by use of Bernoulli's equation far ahead and behind the actuator disk, neglecting the swirl velocity in the duct wake shown in Fig. 1. This procedure gives

$$\gamma/V_0 = (C_{TP(D)} + 1)^{1/2} - \cos\alpha_0 \tag{1}$$

where

$$C_{TP(D)} = \Delta p/q_0$$

3.1 Hovering Thrust Ratio

For hovering flight ($V_0 = q = 0$) the propeller thrust can be evaluated from Eq. (1) as

$$T_{P(D)} = \pi D^2/4\ \rho\gamma^2/2 \tag{2}$$

The ratio of duct to propeller thrust given by the present analysis for hovering is

$$T_{D(P)_h}/T_{P(D)_h} = f_4 \tag{3}$$

where f_4 is given in Table 1 and plotted vs c/D in Fig. 2. For short ducts, Eq. (3) reduces to the limiting value given in Refs. 6 and 7 for $c \ll D$:

$$\frac{T_{D(P)_h}}{T_{P(D)_h}} = \frac{2c}{\pi D}\left(\ln\frac{16D}{c} - 2\right)^2 \tag{4}$$

This result is shown dashed in Fig. 2. Equations (3) and (4) agree within 10% for $c \leq (\frac{1}{4})D$. The asymptotic value of the thrust ratio for $c/D \to \infty$ is unity for a thin cylindrical ducted actuator disk according to simple momentum theory based upon plausible assumptions regarding the slipstream.[2]

3.2 Force and Moment Coefficients at Angle of Attack

For steady flow at angle of attack ($q = 0$) the analysis gives the following static force and moment coefficients for a thin cylindrical duct:

$$C_{ND(P)} = f_1 \sin\alpha_0 \cos\alpha_0\left(1 + \frac{\gamma}{V_0 \cos\alpha_0} f_2\right) \tag{5}$$

$$C_{TD(P)} = f_3 \sin^2\alpha_0 + f_4\left(\frac{\gamma}{V_0}\right)^2 \tag{6}$$

$$C_{m_N})_{D(P)} = f_5 \sin\alpha_0 \cos\alpha_0\left(4 + \frac{\gamma}{V_0 \cos\alpha_0} f_6\right) \tag{7}$$

$$(C_{m_T})_{D(P)} = \frac{\gamma}{V_0} \sin\alpha_0 f_7 \tag{8}$$

The values of the coefficients are given in Table 1 and plotted vs c/D in Fig. 2 together with their limiting values for $c \ll D$ from Ref. 7 which are shown dashed. The latter two equations give the pitching moments about the duct center due to the normal and thrust forces, respectively.

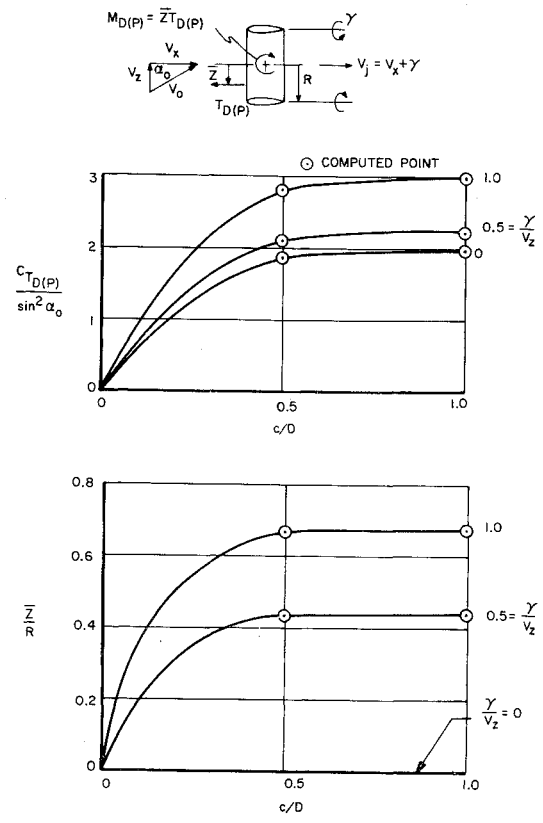

Fig. 4 Duct thrust and center of pressure at angle of attack for a thin cylindrical duct, Eqs. (6) and (8).

The displacement of the duct thrust force from the axis $\bar{Z}$ can be found by division of Eq. (8) by (6) as

$$\frac{\bar{Z}}{R} = 2^{1/2}\left[\frac{V_0 \sin\alpha_0}{\gamma} f_8 + \left(\frac{V_0 \sin\alpha_0}{\gamma} f_8\right)^{-1}\right]^{-1} \tag{9}$$

where f_8 is given in Table 1 and Fig. 2. Similarly the center of pressure of the duct normal force can be found by division of Eq. (7) by (5). The thrust and normal force coefficients for the duct together with their centers of pressure are plotted in Figs. 4 and 5.

3.3 Pitching Stability Derivatives

The force and moment on the duct due to its pitching motion about its own center are given by the following stability derivatives, which are defined in the Nomenclature and Sec. 2.

$$C_{N_q})_{D(P)} = \cos\alpha_0\left(f_9 + \frac{\gamma}{V_0 \cos\alpha_0} f_{10}\right) \tag{10}$$

$$(C_{T_q})_{D(P)} = -\sin\alpha_0 f_{11} \tag{11}$$

$$(C_{mN_q})_{D(P)} = \cos\alpha_0\left(-f_{12} + \frac{\gamma}{V_0 \cos\alpha_0} f_{13}\right) \tag{12}$$

$$(C_{m_{T_q}})_{D(P)} = -\frac{\gamma}{V_0} f_{14} \tag{13}$$

The f_n coefficients in these equations are given in Table 1 and are plotted in Fig. 3 together with their limiting values for $c \ll D$ from Ref. 7 which are shown dashed.

The forces and moments due to pitching from Eqs. (10–13) are additive to those from Eqs. (5–8) at angle of attack. For example, during pure pitch flight, the total normal force coefficient for the duct is

$$C_{ND(P)} = f_1 \sin\alpha_0 \cos\alpha_0 \left(1 + \frac{\gamma}{V_0 \cos\alpha_0} f_2\right) + \cos\alpha_0 \left(f_9 + \frac{\gamma}{V_0 \cos\alpha_0} f_{10}\right) \frac{Dq}{V_0}$$

4. Effect of Circular Camber, Taper, and Thickness

The effects of duct circular camber and taper will be described first for a thin duct. Subsequently, the effect of duct thickness will be discussed. The duct camberline shape is assumed to be such that

$$dr_s/dx_s = R_1 - R_2(2x_s/c) \tag{14}$$

Corresponding duct shapes, shown by the curves in Fig. 6 together with their mirror images, appear to be reasonably representative of those used in practice. The constant R_1 gives linear taper, and R_2 gives circular arc camber. These constants are assumed to be much smaller than unity so that it is permissible to satisfy the boundary condition at the projected cylindrical surface of radius P. The radius of the duct trailing edge is held constant when camber and taper are added, and the increased length of the duct leading edge due to taper is neglected.

4.1. Duct Thrust for Axial Flow

For a duct with camber and taper there are three components of thrust due to 1) leading-edge suction, 2) the surface pressure distribution excluding both leading-edge suction and the pressure jump across the actuator disk, and 3) the pressure jump acting upon the internal duct surface downstream of the actuator disk.

The first two components are independent of the location of the actuator disk within a duct of specified shape. The third component of the duct thrust is maximum when the actuator disk is located at the minimum duct internal cross-sectional area. For this location the disk area and disk thrust are minimum for a fixed disk loading; furthermore, the thrust ratio of the duct to disk is maximum. The thrust coefficient of the duct and the ratio of the duct to disk thrust are plotted in Fig. 7 for various duct shapes, with the actuator disk at the minimum duct cross section, for axial flow, and for a duct chord-to-diameter ratio of one-half. The thrust ratio for hovering flight is also shown in Fig. 8 for $c/D = \frac{1}{2}$ and various values of R_1 and R_2. It can be seen that the duct thrust and the thrust ratio increase with outward taper downstream ($+R_1$) and with inward camber ($-R_2$), particularly when the propeller loading is high so that V_0/γ is small.

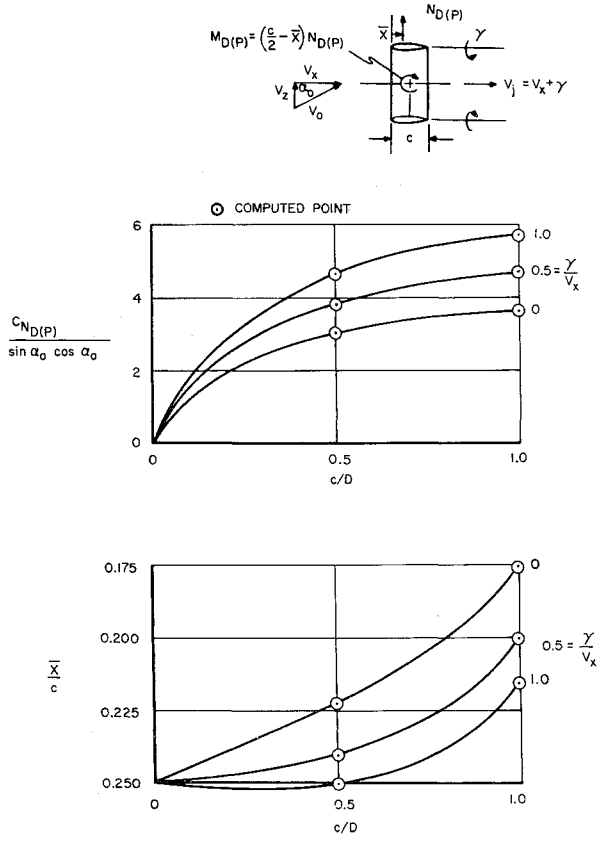

Fig. 5 Duct normal force and center of pressure at angle of attack for a thin cylindrical duct, Eqs. (5) and (7).

4.2. Duct Coefficients and Pitching Derivatives at Angle of Attack

At angle of attack, the effect of small amounts of duct camber and taper upon the duct coefficients and pitching derivatives are shown in Fig. 9. Here, the variation of all of the f_n that depend upon camber and taper are plotted vs V_x/γ, R_1, and R_2 for $c/D = \frac{1}{2}$. Since the only f_n that are affected are those which are multiplied by a γ/V_0 term, there is no effect of taper and camber for a ring wing ($\gamma = 0$). In these results the thrust force and its moment on the duct consist only of the contribution due to leading-edge suction [Eqs. (6) and (8)]. The thrust force and moment due to the axial projection of the duct surface pressure distribution, including the pressure jump across the actuator disk, are not included.

It can be seen that the f_n coefficients are generally more sensitive to taper than circular camber and that the sensitivity to both increases with increasing V_x/γ or with decreasing propeller thrust.

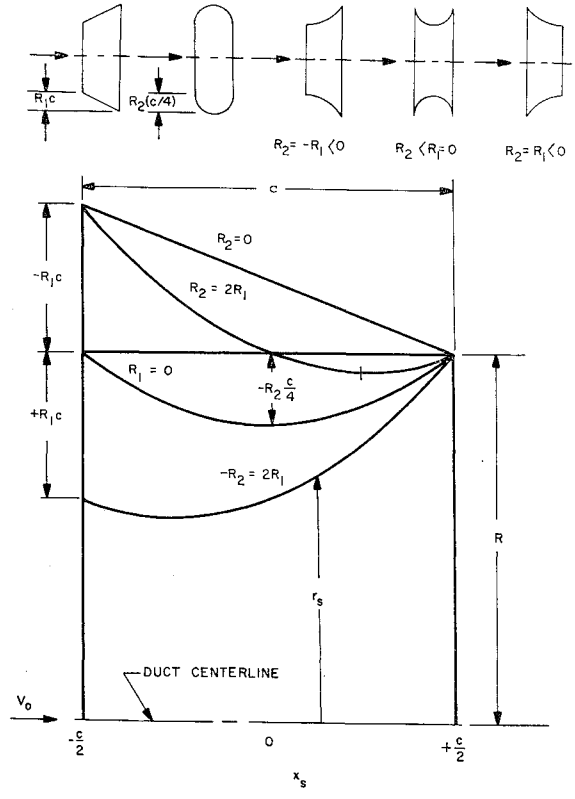

Fig. 6 Duct shapes from Eq. (14).

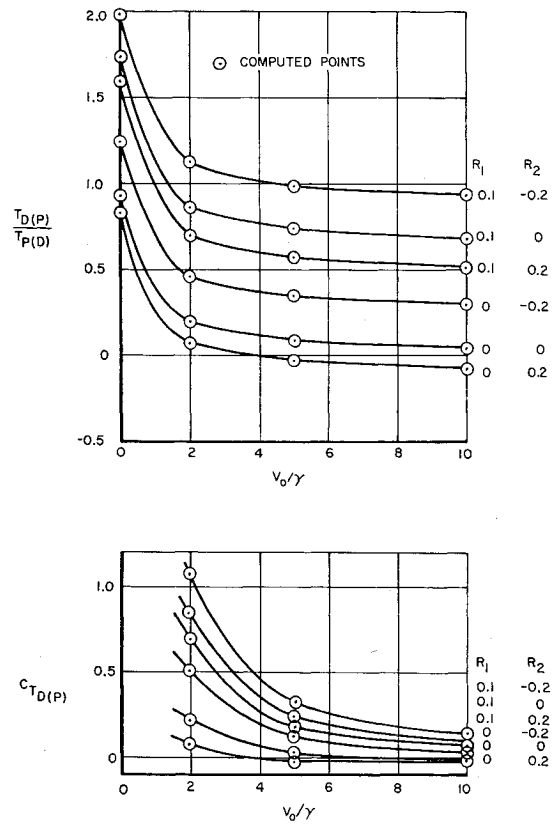

Fig. 7 Duct thrust coefficient and thrust ratio with camber and taper for $c/D = \frac{1}{2}$ and $\alpha_0 = 0$.

As an illustrative example, consider the effects of camber and taper on the normal-force coefficient of the duct for $c/D = \frac{1}{2}$, $\alpha_0 = 10°$, and $\gamma = (\frac{1}{2})V_0$. From Eq. (5) this coefficient is $C_{N_{D(P)}} = 0.171 f_1 + 0.174 f_1 f_2$. For a thin cylindrical duct Table 1 or Fig. 2 gives $f_1 = 3.075$ and $f_2 = 0.530$ so that $C_{N_{D(P)}} = 0.525 + 0.284 = 0.809$. However, for a duct with camber and taper ($R_1 = 0.1$, $R_2 = -0.2$) we obtain from Fig. 9 that $f_2 = 1.081$ and f_1 is unchanged, so that $C_{N_{D(P)}} = 0.525 + 0.579 = 1.104$. Hence, the duct normal force increases 37% because of camber and taper for the assumed conditions.

4.3. Effect of Duct Thickness

Small amounts of duct thickness cause a surface velocity distribution that can be found from Refs. 13 or 14 and added to the distribution previously determined for a thin duct. Examination of the results given in Ref. 13 for a symmetrical Joukowski airfoil with maximum thickness τc and a duct chord-to-diameter ratio of unity indicate the following.

1) The surface velocity distribution generated by thickness is of the same order of magnitude as that generated by the actuator disk and duct-bound vorticity for lightly loaded propellers when $\tau \simeq \gamma/V_0$. However, the effect of duct thickness upon the surface velocity distribution becomes negligible when the propeller thrust coefficient is large and $\tau \ll \gamma/V_0$.

2) The effect of thickness upon the duct leading-edge suction is small. For the above-mentioned ducted propeller using a Joukowski airfoil the ratio of leading-edge suction due to thickness to that without thickness is $0.085\, \tau V_0/\gamma$. Thus, the effect of thickness upon leading-edge suction is negligible unless $\gamma \ll V_0$.

For a ducted actuator disk there is an effect of thickness which does not appear for a ring wing. This is the component of thrust $\Delta T_{D(P)}$ due to the pressure jump across the actuator disk acting upon the projected duct surface area $A - A_p$, such that

$$\Delta T_{(DP)} = \Delta p(A - A_p) \qquad (15)$$

This componet of thrust can be generated by duct camber, taper, or thickness; it can be of significant magnitude for duct shapes used in practice; and the effect due to thickness is simply additive to the results previously obtained neglecting thickness.

The effects of duct thickness upon the static coefficients and pitching derivatives have not been considered. Except for duct thrust, however, the foregoing results indicate that the thickness effects are negligible when the propeller thrust coefficient is large and $\tau \ll \gamma/V_0$.

5. Calculative Example and Comparison with Data

As a calculative example the results given in Secs. 3.2 and 4.3 will be used to predict the forces and moments on the ducted propeller configuration tested by Grunwald and Goodson in Ref. 15. The test configuration is shown in Fig. 10. The propeller had three blades, and the stator had four vanes. The taper and camber of the duct are small and will be neglected, but the effect of internal expansion of the duct due to thickness will be included in the predicted duct thrust. The duct force and moment will be predicted at 20° angle of attack.

For a thin cylindrical duct with chord-to-diameter ratio $c/D = 0.611$ we obtain from Fig. 2: $f_1 = 3.30$, $f_2 = 0.54$, $f_3 = 1.95$, $f_4 = 0.93$, $f_5 = 0.28$, $f_6 = 1.50$, and $f_7 = 1.90$. The propeller thrust coefficient was measured to be $C_{T_{P(D)}} = 0.970$. Using this value we obtain (Eq. (1)) $\gamma/V_0 = 0.465$, and $V_j/V_0 \sin\alpha_0 = \cot\alpha_0 + (\gamma/V_0)\csc\alpha_0 = 4.1$. The latter value indicates that the initial assumption of small cross flow is probably justified for the present example.

Substitution into Eqs. (5–8) gives the predicted force and moment coefficients for a straight thin duct as $C_{N_{D(P)}} = 1.34$, $C_{T_{D(P)}} = 0.442$, and $C_{m_{D(P)}} = 0.730$.

The incremental duct thrust coefficient due to internal expansion of the duct after the propeller, as given by Eq. (15) with Δp from Eq. (1), is $\Delta C_{T_{D(P)}} = C_{T_{P(D)}}(A - A_p/A) = 0.970\ (0.211) = 0.204$ and the total predicted duct thrust coefficient is 0.646.

As a matter of interest, the three predicted coefficients previoulsy noted are from 20 to 30% larger than those measured. Values predicted similarly at $\alpha_0 = 0°$, 40°, 65°, and 90° agree with the measured data within +45 to −15%. The lack of agreement is believed to be due mainly to neglecting swirl in the propeller slipstream in Eq. (1) to evaluate γ/V_0 and also to neglecting the fairing that was added on the upstream side of the duct to prevent flow separation (Fig. 10). However, the initial assumption of small cross flow may have contributed to the lack of agreement also,

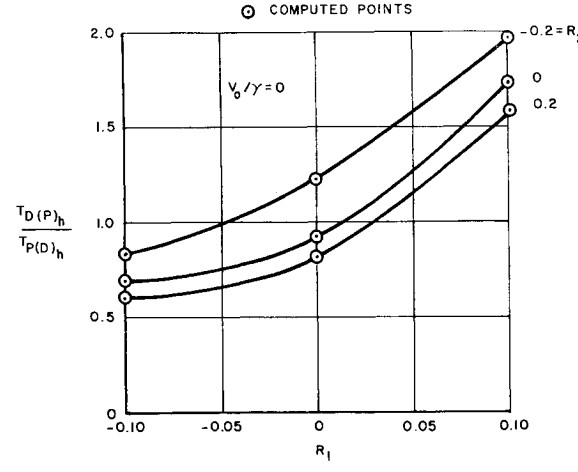

Fig. 8 Thrust ratio with duct camber and taper for hovering flight and $c/D = \frac{1}{2}$.

since $V_j/V_0 \sin\alpha_0$ became as small as 2.1 at the larger angles of attack.

Data were taken by Platt[16] for hovering flight and a ducted propeller very similar to that used in Ref. 15 and shown in Fig. 10. The duct-to-propeller thrust ratio can be predicted from the present analysis including the effect of duct thickness from Eqs. (1, 6, and 15), with $V_0 = \alpha_0 = 0$ and with the measured propeller thrust coefficient. The predicted thrust ratio is 3% lower than measured in Ref. 15 and 7% higher than measured in Ref. 16.

Data were taken by Grose[17] at small angles of attack with a relatively thin and cylindrical duct having a chord-to-diameter ratio of $c/D = 0.475$. The measured lift coefficient of this duct at 6° angle of attack was shown to agree within 1% with the linearized theory for a short cylindrical duct in Ref. 7. Furthermore, the initial assumption of small cross flow was justified since $V_j/V_0 \sin\alpha_0 = 9.1$. The present theory is in good agreement with the linearized theory and the measured data for this ducted propeller.

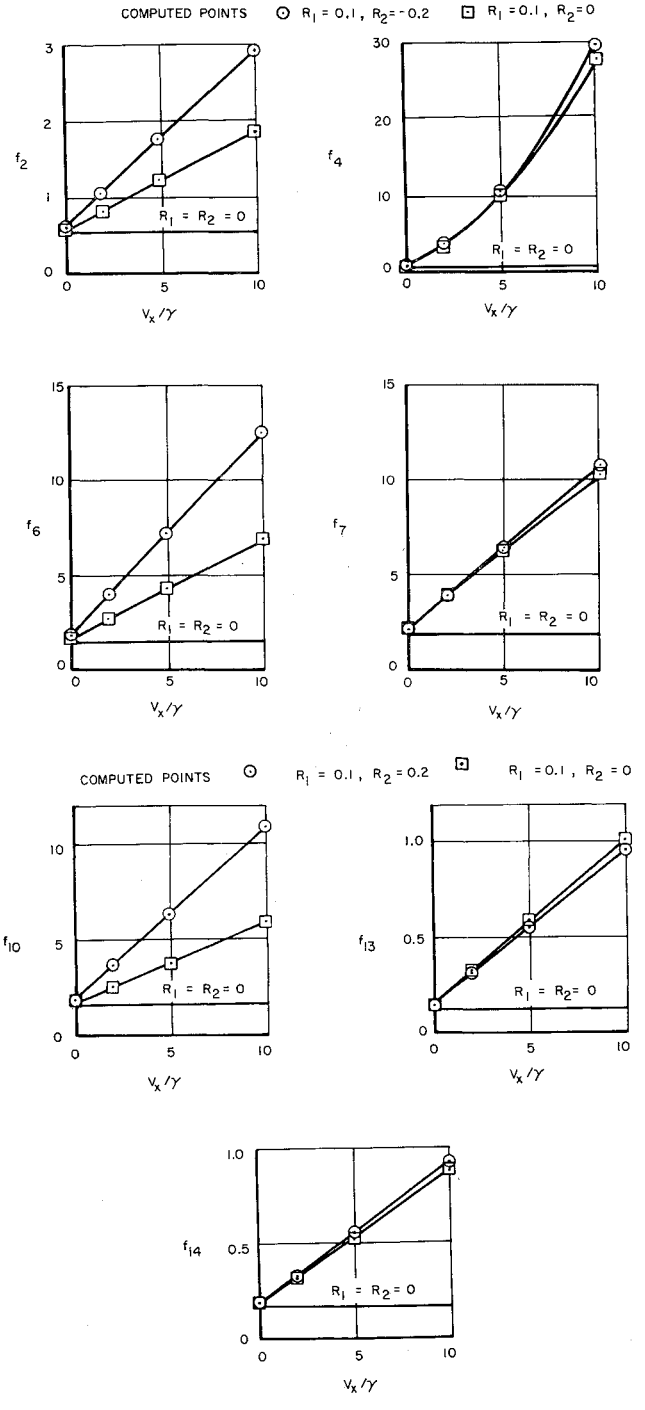

Fig. 9 Computed functions for a thin duct with camber and taper and $c/D = \frac{1}{2}$.

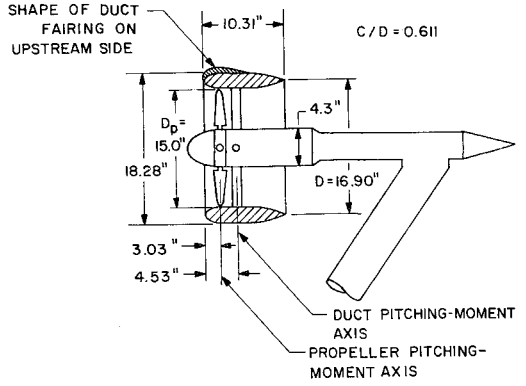

Fig. 10 Ducted propeller configuration tested by Grunwald and Goodson.[15]

In the comprehensive technical report from which the results herein are taken,[18] the static stability and damping in pitch are estimated for VTOL aircraft and torpedo configurations that employ ducted propellers for propulsion. Also, the theory is extended to include a first analysis of the effects upon the duct force and moment of flow interference from an adjacent ducted propeller.

6. Conclusions

The following conclusions are based upon the preceding analytical results for an isolated ducted actuator disk.

1) For hovering flight and a thin cylindrical duct, the duct thrust becomes only slightly less than the propeller thrust when the duct length becomes greater than its radius.

2) For a duct with circular camber, taper, and thickness, the actuator disk should be located at the minimum internal cross section for maximum duct thrust, thrust ratio, and propulsive efficiency. The duct thrust increases with small amounts of thickness, with camber convex inward, and with outward taper downstream.

3) The pitching moment about the center of a thin cylindrical ring wing at angle of attack is due entirely to the normal force and there is no moment from leading-edge suction. The normal force moves slightly ahead of the duct quarter chord with increasing duct chord-to-diameter ratio. The addition of the actuator disk moves the duct normal force aft slightly, but more important, the duct thrust force moves off the centerline by as much as 0.71 of the duct radius causing a large positive pitching moment.

4) The normal force on the duct at angle of attack increases with outward taper downstream and with inward camber.

5) The static coefficients of the duct and the pitching derivatives increase with duct chord-to-diameter ratio. The present results are between 40% lower and 27% higher than those obtained previously for short cylindrical ducts[7] when the chord-to-diameter ratio is 0.4. The agreement is better for shorter ducts and worse for longer ducts. Values generally increase with outward taper downstream, and with inward camber when the propeller thrust coefficient is high.

6) Values predicted by the present analysis are in good agreement with the duct thrust force measured by Platt[16] during hovering flight and the duct lift force measured by Grose[17] at small angle of attack.

7) The present theory, including the effect of duct thickness upon thrust, predicts the duct static coefficients measured by Grunwald and Goodson[15] within +45 to −15% for hovering flight and at angles of attack up to 90°. A significant portion of the duct thrust is caused by internal expansion after the propeller due to duct profile thickness.

8) Frictional drag and real slipstream effects probably must be included in the present analysis either to predict an optimum duct shape or to achieve better over-all agreement with measured data.

References

[1] Dickmann, H. E., "Fundamentals of annular airfoil theory (nozzles in a free stream)," Ingr-Arch. II (1940); transl. by A. B. Finkelstein, L. Meyerhoff, and B. Zacharkiw, as PIBAL Rept. 353, Polytechnic Institute of Brooklyn, Dept. of Aeronautical Engineering and Applied Mechanics, Armed Services Technical Information Agency ASTIA AD 125091 (August 1956).

[2] Sacks, A. H. and Burnell, J. A., "Ducted propellers—A critical review of the state of the art," *Progress in Aeronautical Sciences*, edited by A. Ferri, D. Küchemann, and L. H. G. Sterne (Pergamon Press, New York, 1962), Vol. 3, pp. 85–135.

[3] Morgan, W. B., "A theory of the ducted propeller with a finite number of blades," Univ. of Calif., Institute of Engineering Research, Berkeley, Calif., Ser. 82, Contract Nonr-222(30) (May 1961); also 4th Naval Symposium.

[4] Ordway, D. E., Sluyter, M. M., and Sonnerup, B. O. U., "Three dimensional theory of ducted propellers," TAR-TR-602, Therm Advanced Research, Div. of Therm (August 1960).

[5] Ordway, D. E. and Greenberg, M. D., "General harmonic solutions for the ducted propeller," TAR-TR-613, Therm Advanced Research, Div. of Therm (August 1961).

[6] Burggraf, O., "Aerial jeep phase I," Final Rept., Appendix D, Vol. II, U. S. Army Contract DA-44-177-TC-397, Aerophysics Development Corp. Rept. 520-3/R24/46 (December 1957).

[7] Kriebel, A. R., Sacks, A. H., and Nielsen, J. N., "Theoretical investigation of dynamic stability derivatives of ducted propellers," Vidya Rept. 63-95 (January 1963).

[8] Weissinger, J., "On the aerodynamics of ring wings. I. The pressure distribution of a thin, almost axially symmetric wing in subsonic flow," Deut. Versuchsanstalt Luftfahrt e. V. DFL—Mülheim (Ruhr) (September 1955); also transl. by S. de los Santos, David Taylor Model Basin Aero. Rept. 899, Armed Services Technical Information Agency ASTIA AD 102118 (June 1956).

[9] Weissinger, J., "Remarks on ring airfoil theory," Institute für Angewandte Mathematick der Technischen Hochschule Karlsruhe, European Office Air Research and Development Command, Contract AF 61(514)-1207, Air Force Office of Scientific Research, AFOSR TN 58-224, Armed Services Technical Information Agency, ASTIA AD 154127 (January 1958).

[10] Ladurner, O., "Theoretical investigation by measuring tests in what a degree the economy of flying vehicles is influenced by pre-cambered skeletons of airfoils closed in themselves," Bureau Technique Zbrowski, DA-91-508-EUC 393, Armed Services Technical Information Agency, ASTIA AD 227082 (August 1959).

[11] Küchemann, D. and Weber, J., *Aerodynamics of Propulsion* (McGraw-Hill Book Co., Inc., New York, 1953), Chap. 6, pp. 125–140.

[12] Weissinger, J., "Ring airfoil theory. Problems of interference and boundary layer," Institute für Angewandte Mathematick der Technischen Hochshule Karsruhe, European Office Air Research and Development Command, Contract AF 61(514)-1207, Air Force Office of Scientific Research, AFOSR TN 59-1226, Armed Services Technical Information Agency, ASTIA AD 211809 (January 1959).

[13] Weissinger, J., "The influence of profile thickness on ring airfoils in steady incompressible flow," Institute für Angewandte Mathematick der Technischen Hochschule Karsruhe, European Office Air Research and Development Command, Contract AF 61(514)-904, Air Force Office of Scientific Research, AFOSR TN 57-8, Part II, Armed Services Technical Information Agency, ASTIA AD 120424 (January 1957).

[14] Hough, G. R., "The aerodynamic loading on streamlined ducted bodies," TAR-TR 625, Therm Advanced Research, Div. of Therm (December 1962); also Eighth Midwestern Mechanics Conference, Cleveland, Ohio (April 1–3, 1963).

[15] Grunwald, K. J. and Goodson, K. W., "Aerodynamic loads on an isolated shrouded-propeller configuration for angles of attack from −10° to 110°," NASA TN D-995 (January 1962).

[16] Platt, R. J., "Static tests of a shrouded and an unshrouded propeller," NACA RM L7H25 (February 1948).

[17] Grose, R. M., "Wind tunnel tests of shrouded propellers at Mach numbers from 0 to 0.60," Contract AF 33(616)-5363, Wright Air Development Center TR 58-604, Armed Services Technical Information Agency, ASTIA AD 205464, United Aircraft Corp., Research Dept. (December 1958).

[18] Kriebel, A. R., "Theoretical investigation of static coefficients, stability derivatives, and interference for ducted propellers," Itek Corp., Vidya Rept. 112 (March 31, 1964).